Figures of Merit for Testing Standard Models: Application to Dark Energy Experiments in Cosmology

- A. Amara^{*1} & T. D. Kitching^{†2}
 ¹Department of Physics, ETH Zurich, Wolfgang-Pauli-Strasse 16, CH-8093Zurich, Switzerland
- ² SUPA, Institute for Astronomy, University of Edinburgh, Royal Observatory Edinburgh, Blackford Hill, EH9 3HJ

Accepted —. Received —; in original form —.

ABSTRACT

Given a standard model to test, an experiment can be designed to: (i) measure the standard model parameters; (ii) extend the standard model; or (iii) look for evidence of deviations from the standard model. To measure (or extend) the standard model, the Fisher matrix is widely used in cosmology to predict expected parameter errors for future surveys under Gaussian assumptions. In this article, we present a framework that can be used to design experiments such that it maximises the chance of finding a deviation from the standard model. Using a simple illustrative example, discussed in the appendix, we show that the optimal experimental configuration can depend dramatically on the optimisation approach chosen. We also show some simple cosmology calculations, where we study Baryonic Acoustic Oscillation and Supernove surveys. In doing so, we also show how external data, such as the positions of the CMB peaks measured by WMAP, and theory priors can be included in the analysis. In the cosmological cases that we have studied (DETF Stage III), we find that the three optimisation approaches yield similar results, which is reassuring and indicates that the choice of optimal experiment is fairly robust at this level. However, this may not be the case as we move to more ambitious future surveys.

Key words: Numerical Methods, Cosmology

INTRODUCTION

In cosmology, the Λ CDM concordance model has become our standard model of the Universe. This model satisfies current data and depends on three critical sectors: (i) Dark Energy; (ii) Dark Matter; and (iii) Initial Conditions. These sectors are linked through our theory of gravity - general relativity. Although this model is well defined, the addition of each component has typically been done to explain the available data rather than arising from some fundamental theory of the cosmos. Hence, cosmology is currently in a data-driven era, with little known about the fundamental nature of dark matter and dark energy. As a result, a significant effort is underway in this very active field to build experiments to measure and extend our standard model. These include KIDS, Pan-STARRS¹, DES², LSST³, JDEM⁴

(the ratio of pressure to density of dark energy w(z)) garners the most attentions and is typically parameterised in terms of a second order Taylor expansion in the scale factor or redshift z (e.g. $w(z) = w_0 + w_0 z/(1+z)$). Experiments are then designed to measure these equation of state parameters to the highest possible precision. The dark energy Figure of Merit (FoM; Albrecht et al. 2006), which is proportional to the area of the error ellipse in the w_0 - w_a plane is widely used to gauge performance. Other possible metrics have also been suggested, such as the addition of parameters to test for deviations from Einstein gravity or the division of w(z) into a large number of redshift slices that can then be used to construct principal components through a matrix inversion (Albrecht et al. 2009; Huterer & Starkman 2003). However,

these two suffer from their own problems. For instance, the

additional modified gravity parameters may not be strongly

and Euclid^{5,6}. In planning such future observations, the ap-

proach to date has been to optimise the experimental and methodological designs to minimise the errors on extended

parameters. In particular, the dark energy equation of state

 $^{^{\}star}$ adam.amara@phys.ethz.ch

tdk@roe.ac.uk

http://pan-starrs.ifa.hawaii.edu

http://www.darkenergysurvey.org

³ http://www.lsst.org

⁴ http://jdem.gsfc.nasa.gov

⁵ http://www.euclid-imaging.net

⁶ http://sci.esa.int/euclid

2 Amara & Kitching

motivated and the eigenfunction decomposition of w(z) can suffer from instabilities (Kitching & Amara 2009).

In this article, we present an alternative methodology to be applied to experimental design when faced with a standard model and no guidance from theory. We show that an experiment can be designed such that the probability of breaking the standard model (finding evidence against the model) can be maximised.

This article is organised as follows. In Section 2, we review the alternative approaches to experimental design. We then, in Section 3, compare each approach using a simple explanatory model, as well as a cosmological example that studies the performance of the 'current' and Stage III experiments discussed in Albrecht et al. (2006). We summarise our conclusions in Section 4.

2 APPROACHES TO EXPERIMENT DESIGNING

When planning an experiment with a standard model (a set of parameters) in mind, we can think of three possible approaches that we can take. The first is to stay within the standard model and to design an experiment that will measure the parameters of this model to the highest possible precision. The next is to extend the standard model (add extra parameters), and ideally this extension would be driven by a compelling theoretical framework with clear testable predictions. Finally, in the absence of any compelling theory, one can take a more exploratory approach, where the driving aim is to design an experiment with the greatest chance of breaking the standard model. Ideally, this approach would depend only on well-founded knowledge, such as today's data, the expected error bars of future data and the standard model that is being tested.

2.1 Measuring the Standard Model

Within a well-specified model, the Fisher matrix formalism (Tegmark et al. 1997) is a well-defined framework for estimating the errors that a given experiment will have on the measurement of the parameters of the model. For an experiment where the parameters have an effect on the mean, the Fisher matrix is defined as

$$F_{ij} = \sum \frac{1}{\Delta C^2} \frac{\partial C}{\partial \Theta_i} \frac{\partial C}{\partial \Theta_j},\tag{1}$$

where C is some observable signal, ΔC is the expected error for an experiment and Θ is a vector containing the parameters. A cosmology model may include $\Theta = \{\sigma_8, \Omega_m, \Omega_b, \Omega_\Lambda, n_s, h, \text{etc}\}$, where, for instance, the dark energy equation of state is assumed to be a cosmological constant $(w(z) \equiv -1)$. The errors on each of these parameters

are then given by the diagonal elements of the parameter covariance matrix (Cov), which is given by $Cov = F^{-1}$.

2.2 Extending the Standard Model

When seeking out new physics, we look for ways of going beyond the standard model. Ideally this would be done through the guidance of theory. There are many examples of cases where theories have been put to the test by experiments based on verifiable predictions. One such example is neutrino mass. In the standard model of particle physics, neutrinos have zero mass, but the assumption of zero mass is an ad hoc choice. A natural and physically motivated extension of this model was to add mass to neutrinos (through the lepton mixing matrix addendum). Neutrino mass has now been experimentally confirmed by a number of particle physics experiments (Ahmed et al. 2004; Eguchi et al. 2003; Ahn et al. 2006), and cosmological experiments should be able to constrain this mass to high accuracy (e.g. Refregier et al. 2010; Thomas et al. 2009; Kitching et al. 2008).

Extra parameters, Ψ , can be added to the parameters of the standard model, Θ . In this case, the Fisher matrix formalism can once again be used to estimate the errors on all the parameter sets. Here, it becomes useful to decompose the matrix as

$$F = \begin{pmatrix} F^{\Theta\Theta} & F^{\Theta\Psi} \\ F^{\Psi\Theta} & F^{\Psi\Psi} \end{pmatrix}, \tag{2}$$

where the matrix $F^{\Theta\Theta}$ contains the Fisher matrix elements for the parameters of the standard model, $F^{\Psi\Psi}$ contains the elements for the new model parameters and $F^{\Theta\Psi}$ contains the cross terms.

This approach has been widely adopted by the cosmological community in dark energy studies. In this case, the extra parameters are typically added in the form of equation of state parameters (the ratio of pressure to density) of dark energy (w). However, this is a specific way of thinking about dark energy (as a dynamical fluid). Therefore, models that do not treat dark energy as a fluid have to work in terms of an 'effective' equation of state. A further complexity arises because the observed low redshift acceleration that motivates dark energy could result from other physics, such as the breakdown of Einstein gravity on cosmic scales. A move away from Einstein gravity may not be well represented by the addition of equation of state parameters and may require the addition of new parameters that specifically allow for such deviations. As a result, these extra dark energy parameters do not have a firm theoretical basis but are, in fact, an arbitrary expansion of the equation of state (Kitching & Amara 2009).

2.3 Breaking the Standard Model

Here, we introduce a new approach to experimental planning, where we explicitly design an experiment to maximise the probability of finding a deviation from the standard model. This deviation is allowed to come from any part of the theory and should not depend on any particular theoretical extension of the standard model. The robustness of such an approach can be achieved by relying on minimal inputs, namely: (i) current data; (ii) expected error bars of future measurements; and (iii) the standard model that we want to test.

We begin by defining some basic parameters. Let X be a data vector containing today's measurements (for instance a correlation function). These data points have associated errors, σ_X^2 , which means that the measured data points are randomly scattered about T, the data vector that would be measured with no measurement error or systematic, i.e. the underlying values of the observable as measured with the perfect experiment⁷. The expected error bars of a future experiment are σ_Y^2 , which would produce a data vector Y. Given today's data, we can calculate the probability of the future data, P(Y|X), by marginalising over T,

$$P(Y|X) = \int P(Y|T)P(T|X) dT,$$
 (3)

where P(T|X) is the probability of T given today's data and P(Y|T) is the probability of the future data given T. The integral is performed over all possible T since we do not know what T is a priori.

For each realisation of the future data, there will be an associated best-fit that can be achieved with the standard model. We focus here on the χ^2_{\min} . With the probability distribution of future data given current data (P(Y|X)), which, for simplicity, we will sometimes also denote using P(Y), we can calculate the expectation value of the minimum χ^2 by integrating over all possible future data vectors:

$$\langle \chi^2_{\min} \rangle = \int \chi^2_{\min}(Y) P(Y) \ dY.$$
 (4)

A high χ^2_{\min} means that the standard model is not able to give a good fit to future data. Hence, an experiment designer who wants to maximise his or her chances of breaking the standard model should focus on an experiment configuration that maximises the expectation value of the minimum χ^2 ; max[$\langle \chi^2_{\min} \rangle$]. Strictly, we should use a quantity that is robust to the number of data points (for instance the reduced χ^2). We avoid such problems in what follows by only

making comparisons between experiments with equal numbers of data points. The χ^2 and reduced χ^2 are, therefore, simply scaled versions of each other. In this work, we have focused on the expectation value of the minimum χ^2 of the future data, with the understanding that a χ^2 corresponding to a reduced χ^2 significantly larger than one will require additional parameters beyond those available in the standard model. However, it may be interesting to also consider the higher order statistics of the minimum χ^2 distribution. Along similar lines of thought, our FoM could also be recast in terms of the probability that a future experiment will give a $\chi^2_{\rm min}$ greater than some threshold value. For the work presented here, we use the simplest expression (given in equation 4), but we are continuing to investigate further possible expressions of this model breaking FoM.

Here, we use the maximum likelihood fit to the data (minimum χ^2). We have used this frequentist measure, as opposed to a Bayesian evidence criteria, because there are no objective Bayesian measures in the case of assessing the quality of a theoretical fit for a single model, given that a single model Bayesian evidence must conclude (through a normalisation of probabilities) that there is 100% evidence for that model (see Taylor & Kitching, 2010 for further discussion). In general, this $\chi^2_{\min}(Y)$ measure could be replaced with any 'goodness of fit' criteria G(Y), where equation 4 optimises fit

3 APPLICATION

3.1 Illustrative Example

In Appendix A, we explore the impact of the choice of optimisation metric on a simple illustrative example. We set up a system of three data points and 'a standard model' that is a straight line with one degree of freedom - the slope of the line. What this shows is that the optimal configuration of a future experiment can vary drastically and can lead to exactly opposite optimisations in some cases depending on whether model breaking or standard model extension is used.

The simple model that we set up has a 'pivot point,' where the model makes an exact prediction, $C(x=8) \equiv 10$. To measure the standard model parameter (the slope), assuming that this model is correct, it is clear that there is no sensitivity at this point. Therefore, an optimisation will minimise future error bars away from the pivot point. However, in the model breaking mode, it is optimal to place the smallest future error bars at the pivot point, since it is here that even the slightest deviation from the standard model prediction would yield proof that the standard model is broken. Of course the model breaking paradigm here is a high-risk, high-gain approach. If T happens to have the same value as that of the pivot point, then this approach would yield no extra information. When extending the standard model, the optimal configuration is entirely dependent on the exact form of the extension. For instance, a clear difference is seen

⁷ As an example, if X is calculated from the mean of n independent data points and the errors are given by the variance $(\sigma^2(\bar{X}) = \sigma^2(X)/n^2)$, then T would be the measure given as n goes to infinity in the absence of systematics. We note that, in this case, cosmic variance would come from the fact that due to a finite Universe the number of independent data points will be limited to a finite number.

4 Amara & Kitching

between a standard model that is extended by adding a constant parameter and one that is expanded with a parabolic term about the pivot point, thereby preserving the pivot point.

3.2 Cosmological Application

We now apply our approach to investigate the planning of cosmology surveys. In this work, we focus on some simple examples that show how this can be done, with a more complete investigation of future surveys to follow in later work. In this example, we focus on supernovea (SNe) (Tegmark et al. 1998) and Baryon Accoustic Oscillation (BAO) (e.g. see Rassat et al. 2008, for discussion). In addition, we will show: (i) how external data, in this case the CMB peak separation, can be added; (ii) how priors coming from theory can be included; and (iii) a simple treatment for systematics errors.

3.2.1 Survey Configurations

Due to the computational limits of performing the integral shown in equation 4, the dimensionality of which scales with the number of data points, we have decided to bin the low redshift data (i.e. SNe and BAO) into four redshift bins (i. 0.1 < z < 0.4; ii. 0.4 < z < 0.7; iii. 0.7 < 1.0; and iv. 1.0 < z < 1.3). By fixing the number of redshift bins, and therefore the number of degrees of freedom since the standard cosmology model is the same for all cases, we are able to compare the χ^2_{\min} values directly. This simplifies the comparison between different survey configurations. For current BAO data, we use the galaxy number counts presented in Percival et al. (2010). This work presented a BAO analysis of the Sloan Digital Sky Survey Data Release 7 sample (DR7). This is composed of roughly 900,000 galaxies over 9100 deg^2 in the redshift range z = [0.0, 0.5]. We rebinned this data into our four redshift bins which leads to the distribution shown in Table 1. For current SNe data, we use the Union data presented in Kowalski et al. (2008). This is a compilation of SNe data coming from a number of measurements, including the Supernova Legacy Survey, the ESSENCE Survey and supernovae measurements from the Hubble Space Telescope (HST). Once again, as with the BAO data, we have re-binned this data to match the four bins that we use in this paper (see Table 2). As we will discuss in Section 3.2.2, we have also included constraints coming from current measurements of the CMB peak separation presented in Komatsu et al. (2009), which uses the WMAP data.

For future surveys, we have decided to focus on a configuration that illustrates the technique presented here, rather than to make concrete recommendations about specific mission concepts. The reason for this is that the calculations that we present here include a number of simplifications, such as using only four redshfit bins. These, we feel, allow us to calculate trends and make some statements about the

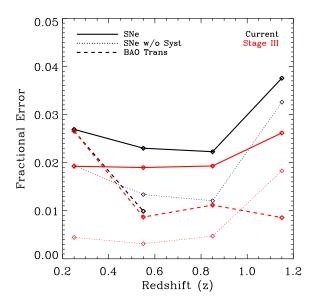


Figure 1. Fractional errors on the observed quantities for 'current' (black) and stage III (red) experiments. For the BAO measurements, these are the errors on the transverse BAO scale from Blake et al. For the SNe surveys, the observable is the flux loss of the SNe.

relative merits of broad concept ideas. However, to draw detailed conclusions on specific mission configurations would take further detailed work that we will address in follow up publications on this topic. For the future surveys that we use to illustrate our method we have relied on the Stage III surveys described in Albrecht et al. (2006), although many of the projects may have evolved since this document was released. Once again, we re-bin the Stage III data into our four redshift bins (see Tables 1 and 2).

For the BAO surveys, we simplify the analysis by only using the tangential modes, which is pessimistic, and assume no systematics, which is optimistic. Due to these reasons, the results below are illustrative, and we do not claim that the optimistic and pessimistic approaches cancel out each other. We calculate the errors on BAO scale using the fitting function given in Blake et al. (2006), which has been implemented in iCosmo (Refregier et al. 2008; Kitching et al. 2009). For the Supernova error calculations, we have used the Fisher matrix approach outlined in Tegmark et al. (1997) and Huterer & Turner (2001) and have assumed a systematic contributions outlined in Kim et al. (2004) and Ishak et al. (2006). However, we will also show results without systematics in order to gauge their impact.

3.2.2 Including External Data

In this study, we focus on the potential of future BAO and SNe surveys. It is, however, straightforward to include other data sets. To do this, we must decide whether to only include current measurements (for instance, in the case of the CMB to include WMAP data) or try and anticipate the joint im-

	Area	Number Density of Galaxies (ng) [num/amin ²]			
		0.1 < z < 0.4	0.4 < z < 0.7	0.7 < z < 1.0	1.0 < z < 1.3
Current	10000	0.013	0.00056	0.0	0.0
Stage III WiggleZ	1000	0.0	0.022	0.089	0.0
Stage III BOSS	10000	0.014	0.019	0.0	0.0
Stage III WFMOS	2000	0.0	0.056	0.22	0.18

Table 1. Parameters of the BAO surveys considered in this study. The current survey is chosen to be close to the BAO survey parameters for the SDSS DRL7 (Percival et al. 2010). The future surveys have been chosen from the Stage III surveys of the Dark Energy Task Force report (Albrecht et al. 2006).

	Number of Supernovae (n _s)					
	0.1 < z < 0.4	0.4 < z < 0.7	0.7 < z < 1.0	1.0 < z < 1.3		
Current SNe	51	107	131	18		
Stage III SNe	965	1940	860	57		

Table 2. Parameters of the Supernovae surveys considered in this study. The current survey is chosen to be close to the Union supernovae sample (Kowalski et al. 2008). The future surveys have been chosen from the Stage III surveys of the Dark Energy Task Force report (Albrecht et al. 2006).

pact of future measurement of that probe (for instance, to include predictions for Planck⁸). If the latter is desired, then the prescription for doing so follows the same logic as that used for the BAO and SNe calculations and would increase the data vectors (F and X) in equation 4. While conceptually simple, adding external data in this way can quickly lead to computational challenges, since the dimensionality of the integral scales the number of data points. The computation time for convergent results can diverge quickly, even using a simple Monte-Carlo integration scheme. To solve potential problems, we would either need to develop a sophisticated Monte-Carlo integration scheme with, for instance, importance sampling that is tailor made for this problem or try to reduce the number of data points by focusing on specific features of the external data that we wish to consider. For instance, in the case of the CMB we can consider adding the peak position and height information rather than implementing the full correlation data $(C(\ell))$.

If we only add existing external data, then the calculation is greatly simplified, since the dimensionality of the integral in equation 4 remains the same. Instead, the external data is simply used when calculating the minimum χ^2 . In the work presented here, we have included the measured spacing of the acoustic oscillation peaks of the CMB, ℓ_A , which depends on the ratio of angular diameter distance to the sound horizon at photon decoupling epoch (z_*) ,

$$\ell_A = (1 + z_*) \frac{\pi D_A(z_*)}{r_s(z_*)},\tag{5}$$

where D_A is the angular diameter distance and r_s is the sound horizon. This peak spacing has been measured to be $\ell_A = 302.1 \pm 0.86$ for WMAP (Komatsu et al. 2009), which gives an expression for z_* in equation 66. For the sound

 8 http://www.rssd.esa.int/SA/PLANCK/docs/Bluebook-ESA-SCI(2005)1_V2.pdf

horizon calculation, we follow the calculations presented in Appendix A of Parkinson et al. (2007).

3.2.3 Theory Priors and Calculating Probabilities

We now turn our attention to priors coming from our theory and how these can bound our results. For example, if we impose no knowledge at all about what we expect, then the PDFs for each of the data points in equation 3 are independent. A simple consequence of this is that the probability distribution for future data in bins where no current data exists (P(F|X)) will be flat between $-\infty$ and ∞ . Inputing this PDF into equation 4 would lead to a $\langle \chi^2_{\min} \rangle$ of infinity, which is not fully useful when comparing expected performances. One can view this result in two ways. The first is that a data purist (i.e. someone who wishes not to add any bounds from theory) would conclude that the best surveys are those that explore new regions where no measurements have yet been made. The alternative approach is to introduce some expectation from our knowledge of basic cosmological theory. Theory priors modify the PDFs of future data by imposing relationships between different data points. A simple addition is to impose a link between the angular diameter distance and the luminosity distance.

For the configurations shown in Table 1, we immediately see that if we take no guidance from theory then we will be driven towards WiggleZ and WFMOS (see Table 1), since these two surveys will provide BAO measurements at redshifts that are currently not explored by current BAO experiments and, hence, have an expectation value of minimum χ^2 of infinity. Once again, a data purist may argue that these surveys should, therefore, be our top priority. In contrast, another simple approach is to rely on the widely accepted relationship between angular diameter distance (D_A) and luminosity distance (D_L) given by

$$D_L = (1+z)^2 D_A. (6) \sigma_c^2 = \frac{\sigma_X^2 \sigma_Y^2}{\sigma_Y^2 + \sigma_Y^2}. (10)$$

By explicitly adding this very weak prior from the theory, the probability of future data is modified (equation 3) to

$$P(Y|X) = \int P(Y_B|D_L)P(Y_S|D_L)P(D_L|X_B)P(D_L|X_S) dD_L,$$
 (7) data have $X_c = X$ and $\sigma_c = \sigma_x$. With this combined data vector, we then calculate γ^2 .

where Y_B and Y_S are the data vectors for future surveys for BAO and SNe (respectively) and X_B and X_S are the data vectors for today's surveys. This PDF, therefore, includes a relationship between the SNe measurements and the BAO measurements at any given redshift. For what we present later, this relationship between distances is the only information that we impose from theory. However, a natural question is what would happen if the future data were to extend to redshifts that are not covered by either the BAO or the SNe data? A detailed exploration of this will be presented in follow-up work. Nonetheless, here we give a brief discussion of the basic principles. Once again, priors from theory can be used to impose relationships between different data points, which in turn modify the PDF of the future data. In particular, the question raised here would look for relationships between data points at different redshifts. This can be done by introducing an integral relationship between distance (co-moving - D_c) and the Hubble function, H(z),

$$D_c = c \int_0^{z'} \frac{dz'}{H(z')},\tag{8}$$

where c is the speed of light. Without resorting to the Friedmann equation, which links H(z) to density parameters of the matter-energy components of the Universe, we can place simple constraints on the functional form of H(z) that can be used to compute the probability of future data. For instance, an assumption that H(z) is a positive definite function over cosmic time would bound the comoving distance at a redshift of z_i to be between the comoving distances at z_{i-1} and z_{i+1} , i.e. that of the redshifts on either side. Here the inclusion of the CMB, with $z \sim 1100$, becomes very useful. The advantage of this approach is that all knowledge from theory, including simple relationships, such as that between D_L and D_A , must be included explicitly. This then allows us to decide explicitly what assumptions should be included.

3.2.4 Computation of $\langle \chi^2_{\min} \rangle$

For each realisation of the the future data (Y) we calculate the weighted average data, which is given by

$$X_c = \frac{\sigma_X^2 Y + \sigma_Y^2 X}{\sigma_Y^2 + \sigma_Y^2},\tag{9}$$

where X_c is the value of the combined data, Y and X are the future and current data values, and σ are the associated errors. The errors on the combined data are

The data vector X_c can also contain external data for which there will not be corresponding future measurements. In this case, the data vector enteries that correspond to the external data have $X_c = X$ and $\sigma_c = \sigma_x$. With this combined data vector, we then calculate χ^2 ,

$$\chi^2 = \sum \frac{(X_c - M)^2}{\sigma_z^2},\tag{11}$$

where the sum is over the entries of the data vector. In our case, this corresponds to a total of nine data points (BAO scale at four redshifts, SNe at four redshifts and the CMB peak spacing). For a given choice of cosmology parameters, M is the value given by the model. For each integration step, we use a minimiser to find the parameters that lead to the smallest χ^2 value.

The Stage III surveys will look for deviations from the standard Λ CDM concordance model. We consider the standard cosmological model as one with Gaussian initial conditions⁹ following inflation, with scale-free perturbations $(n_s = 1)$, where spatial curvature is allowed and dark energy is understood to come from the cosmological constant Λ (i.e. w = -1). Since we only consider the distance-redshift measurements, we are sensitive to the following parameters of the model¹⁰: $\{\Omega_m, \Omega_\Lambda, h\}$. The model breaking approach does not rely a adding further parameters beyond these well-understood ones and will test how likely it is that future experiments, based on today's data, would find any deviation from Λ CDM, including, for example, evidence for $w \neq -1$.

We perform the integral in equation 4 over all possible realisations of the future data, which corresponds to an eight dimensional integral (four future BAO and four future SNe). For practical reasons to do with computational feasiblity, we use the simple Monte-Carlo integration technique outlined in section 7.7 of Numerical Methods (Press et al. 2007). Here, a multidimensional integral (in our case, equation 4) can be expressed as

$$\int f dV \approx V \langle f \rangle \pm V \sqrt{\frac{\langle f^2 \rangle - \langle f \rangle^2}{N}},\tag{12}$$

where the expectation values, denoted by the angular brackets, can be calculated by randomly sampling the function f at positions x_i with

$$\langle f \rangle \equiv \frac{1}{N} \sum_{i=0}^{N-1} f(x_i). \tag{13}$$

 9 See Amara & Refregier (2004); Desjacques & Seljak (2010); Pillepich et al. (2010) for examples of how non-Gaussian initial conditions impact observables at low redshifts

¹⁰ We note that there is a weak dependence on Ω_b through z_* , but we have neglected this here since it has little impact on the results and only complicates the calculation.

The volume of the parameter space is denoted as V. This is set by the bounds of the integral, which we have choosen in such a way as to ensure that the integrand is vanishingly small at this limit.

3.2.5 Results

Performing survey optimisations for future experiments typically involves a trade-off between different configurations that compete for resources. A classic example is a trade-off between the depth and area of a survey for a fixed exposure time (see Amara & Réfrégier 2007, for an example of this for weak lensing surveys). Another, more difficult and often controversial trade-off study, is to trade-off resources between different proposed probes. For instance, if due to limited resources it is not possible to support both SNe and BAO missions envisioned for stage III. A natural question might be - should we invest in one over the other? Or should scaled-down versions of each mission be pursued? This is a complex issue for a number of reasons, but the model breaking figure of merit, along with other FoMs, can help guide such decisions by quantifying the likelihood of finding a deviation from 'the standard cosmological model'. For this reason, our first illustrative example focuses on a possible trade-off study between SNe and BAO stage III surveys. We note again that a thorough treatment of such a trade-off is complicated. For instance, quantifying the impact of limited resources is significantly more complicated than that of limited observation times. We made a number of simplifying assumption, so the results stated here are only to illustrate the method rather than to offer concrete recommendations about one experiment over another. In this spirit, we will show results for the full Stage III surveys, as well as for the scaled down versions. We do not attempt to make a link between the scaled-down versions for a fixed set of resources, since this is well beyond the scope of this work. For scaling down the surveys, we have decided to fix the distributions in redshifts (i.e. the PDF of the number of SNe and galaxies as a function of redshift is fixed), and we vary an overall scaling. For BAO this corresponds to a change in survey area, and for SNe this corresponds to a reduction in the total number

In Figure 2, we show the expectation value of the minimum χ^2 when we consider only some fraction of the area of the Stage III surveys shown in Table 1. For instance, for a fraction of 0.5 we divide the areas of all the BAO missions by a factor of 2. The results are shown for different realisations of Stage III SNe surveys, where once again the fraction refers to the fraction of the total SNe numbers shown in Table 2. We see that for a range of SNe stage III configurations increasing the area of the BAO survey from 1% to 10% of what is expected in stage III has no effect on the expectation value of the minimum χ^2 . Beyond this, however, we see a large increase in $\langle \chi^2_{\rm min}$ as the area of the BAO surveys is increased, leading to mean χ^2_{\min} values that are greater than 5 (i.e. a reduced χ^2 greater than one) for all survey configurations with 100% of the DEFT stage III survey area. This is true with and without SNe systematics. In Figure 3, we show similar results as a fraction of future SNe sur-

	$\langle \chi_m^2 \rangle$	$\sigma_c(\Omega_\Lambda)/\sigma_{III}(\Omega_\Lambda)$	$\rm FoM_{\rm III}/FoM_{\rm c}$
BAO III	5.5	10	2.2
SNe III	3.5 (4.0)	6 (14)	1.1 (2.6)
BAO & SNe III	7.0 (8.0)	10 (19)	2.2 (4.4)

Table 3. Comparison between the model breaking approach $(\langle \chi^2 \rangle)$, working within the standard model (here we show errors on Ω_{Λ} in a model with only cosmological constant) and DETF FoM (which involved parameterising the equation of state in terms of w_0 and w_a). The numbers in parentheses are when no systematics are included for SNe, while the other numbers have this systematic included.

veys. We see linear rise in $\langle \chi^2_{\rm min} \rangle$ with the SNe fraction from 1% to 100% of stage III experiments. Here, the rise is less dramatic than in the BAO case, and this suggests that it is more likely for discovery to come from the BAO experiment. This result can also be seen in Table 3, where we also show the comparison with the other figures of merits discussed in sections 2.1 and 2.2. The middle column shows the errors on the standard model parameters, in this case the density of Λ , and on the right we show the FoM proposed by the DETF, which is proportional to the area of the error ellipse in the w_0 - w_a plane Albrecht et al. (2006). Reassuringly, all three measures show similar trends, which would suggest that the simple optimisations done here are reasonably robust and the overall information content is increased between experiments with lower FoM and ones with higher ones. This is different from the tradeoff studied in appendix A, where the overall error bars are fixed and the sensitivity in different regions (x values) leads to changes in the FoMs.

Finally, we investigate a simple optimisation where we explore the model breaking redshift sensitivity of the Stage III surveys. We do this by boosting the performance of the surveys at a particular redshift by dividing the statistical errors at that redshift by a factor of 2. This is not a physically motivated optimisation. Instead, it can be thought of as simply probing where an improvement would be the most effective. The results are shown in Figure 4. The coloured bars show the fractional increase in $\langle \chi_m^2 \rangle$ for the calculations where SNe systematics have been included. We see here that improving the SNe survey in the two lowest redshift bins causes a notable increase in the $\langle \chi^2_{\rm min} \rangle$, while improving the SNe performance in higher redshift bins has little effect, except in the no systematics case. This suggests that to go beyond stage III SNe experiments we should focus on improving errors at low redshifts first, unless we can demonstrate that the systematics levels can be brought below those presented by Kim et al. (2004) and Ishak et al. (2006). For the BAO experiments, we find a different result. Improving the errors in our lowest redshift bin has no effect on $\langle \chi^2_{\min} \rangle$. However, we see that if the errors in our final redshift bin (0.7 < z < 1.0)are improved, then we see the largest rise in $\langle \chi^2_{\min} \rangle$. This suggests that a BAO experiment beyond stage III should aim to make measurements at high redshifts.

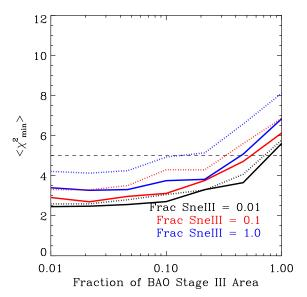


Figure 2. Expectation value of the minimum χ^2 as a function of the areas of the stage III BAO surveys. The fraction corresponds to the fraction of the full survey areas (shown in Table 1) used. These are shown for three configurations of stage III SNe surveys, where only a fraction of the SNe in Table 1 are used. The solid curves include SNe systematics while the dotted curves do not. The dashed line shows the χ^2 that would correspond to a reduced χ^2 of 1.

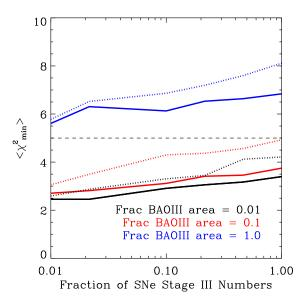


Figure 3. Expectation value of the minimum χ^2 as a function of the number if SNe of the stage III surveys. The fraction corresponds to the fraction of the full survey number (shown in Table 1) used, where the PDF is fixed and only a global fraction is applied. These are shown for three configurations of stage III BAO survey area where only a fraction of the areas in Table 1 are used. The solid curves include SNe systematics while the dotted curves do not. The dashed line shows the χ^2 that would correspond to a reduced χ^2 of 1.

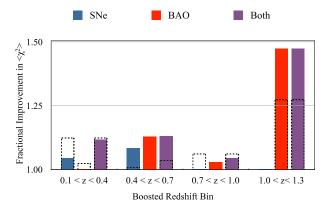


Figure 4. The impact of boosting the performance in one of the redshift bins. This is done by reducing the statistical error in the relevant bin by a factor of 2. The y-axis shows the ratio of the expectation value of the minimum χ^2 of the boosted stage III survey relative to the standard stage III survey. The different colours corresponding to which probe have been enhanced; the solid colours are when SNe systematics are included, and the dashed lines show the results when SNe systematics are eliminated.

4 CONCLUSIONS

We have presented a framework in which experimental optimisation can be placed. Given a standard model, one can either (i) measure the standard model parameters to high precision; (ii) attempt to extend the standard model; or (iii) attempt to find deviations from the standard model.

When designing an experiment to measure or extend the standard model, the Fisher matrix formalism can be used. We have introduced a framework that can be used to design an experiment to have the best chance of finding discrepancies with the standard model. This framework only depends on three sets of information (current data, future expected error bars and the standard model). No external assumptions are needed for the calculations, though we have also shown how priors from the theory can, if needed, be added.

By using a simple illustrative example, we find that the optimal future experiment configuration can depend very strongly on the choice of optimisation metric. In our simple model, C=m(x-8)+10, the data position x=8 is a pivot point since $C(x=8)\equiv 10$. When designing an experiment to measure the standard model, it is optimal to have small errors away from the pivot point. However, when designing an experiment to break the model, it is optimal to have a small error at the pivot point since any measurement of $C(x=8)\neq 10$ would provide evidence that the standard model was incorrect. When extending the model, the optimisation naturally depends on the exact parameterisation of the extension.

In cosmology we have a standard model, Λ CDM. A large number of experiments have been designed to measure an ad hoc extension of this model, parameterisations of the dark energy equation of state, to high accuracy. Our recommendation here is that future cosmology missions should be optimised by using the three approaches we have out-

lined above: (i) measure the standard ΛCDM parameters; (ii) measure extended parameters, specifically the equation of state parameters, the DETF FoM and the modified gravity parameter γ ; and (iii) calculate the expectation value that the experiment will find a deviation from Λ CDM. We calculate quantities in these three regimes for SNe, BAO (transverse modes) and the CMB peak positions by focusing on 'current' and the DETF stage III surveys. Should the three quality quantifiers agree, then we can be reassured that the optimisation is somewhat robust. For instance, there has been some concern that the DETF FoM is biased in favour of redshifts. However, in the calculations shown in this paper, we do not find evidence for this, with the results for the DETF FoM being consistent with the other figures that we have shown. In the event that the three approaches lead to conflicting configurations, the the fact that these measures look for distinctly different thing means that we should be able to make a choice based on a judgement of the priorities of a given experiment.

ACKNOWLEDGMENTS

We would like to thank Alexandre Refregier for the useful and insightful discussions that initiated this work. We also thank Andy Taylor, Fergus Simpson and Anais Rassat for useful comments. AA is supported by the Zwicky Fellowship at ETH Zurich. TDK is supported by STFC rolling grant number RA0888.

APPENDIX A: ILLUSTRATIVE EXAMPLE

To illustrate the distinction between the three optimisation approaches highlighted in this article, we will present a simple worked example. We begin with a standard model where the signal C at x depends only on the parameter m (i.e. $\Theta = \{m\}$). Our standard model is that

$$C = m(x - 8) + 10. (A1)$$

For this simple example, we also assume that measurements can only be made at $x=\{4,8,12\}$, where today's measurements have yielded $X=\{10,10,10\}$ with Gaussian errors of variance $\sigma_Y^2=\{1,1,1\}$. This is shown in Fig. A1. We will assume that future experiments can be built to measure the signal at the same x positions as today but that the errors on the measurements will be significantly smaller than those of today. Specifically, we will assume that the quadratic sum of the future errors, over all data points, is $\sum_x \sigma_Y^2(x) = 2.01$ (this creates a symmetry between the top left and right corners of Figures A2, A3, A4 and A5). The global performance of the future experiment is, therefore, a little better than the current one, and the optimisation process is to decide how to optimally distribute the errors among the three data points.

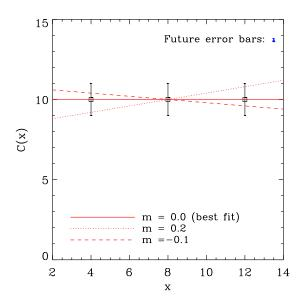


Figure A1. The system being used to illustrate the available optimisation options. For this example, the black points are to-day's data and the red lines are examples of our standard model that are consistent with today's data. In the top right hand corner, an example of the typical size of the error bars in the future experiment is shown.

A1 Measuring the Standard Model

To measure performance of a future experiment, we use the Fisher matrix to estimate the errors on the parameter m for specific configurations of the errors. This allows us to find the optimal configuration of the errors for the purpose of measuring m.

Fig. A2 shows how the future errors at the x=4 and x=8 points are optimised such that the error on m is minimised. It is clear that the optimal configuration is insensitive to the error at x=8. This is understandable since within the standard model there is not sensitivity to m at x=8, so there is no gain in placing any measurement at this point. The optimal strategy to measure the standard model m is then to place small future error bars at either x=4 or x=12. It is also interesting to note that since the value of the standard model at x=8 is fixed, it is better to have one small error on either x=4 or x=12 (with the other being large) than to distribute the errors between these two points.

A2 Extending the Standard Model

To extend the model, we first have to decide on a way of extending the standard model. We must also decide whether to optimise or minimise the errors on the extended parameters - after marginalizing over m - or to minimize both the standard and extended parameters simultaneously.



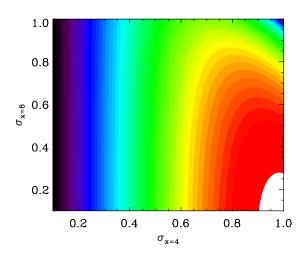


Figure A2. The results of an optimisation analysis designed to measure m (the only parameter of our standard model) to the highest precision possible. The quadratic sum of the errors of the three data points, $(\sigma_{x=4}^2 + \sigma_{x=8}^2 + \sigma_{x=12}^2)$, has been set to 2.01. We see that the minimal errors are achieved for small $\sigma_{x=4}^2$ (and by symmetry $\sigma_{x=12}^2$). The fact that the lines are close to vertical shows that this optimisation is totally insensitive to the measurement precision at x=8. This can be understood since x=8 is a pivot in our standard model and therefore offers no information within our standard model since it can only have a value of 10. For a fixed error at x=8, we see a clear preference to mimise the errors at either x=4 or x=12, which means that it is better to have one small error bar than mimising both.

For illustration, we assume that there are two equally valid ways of extending the standard model used here. The first is the addition of a quadratic term,

$$C = m(x-8) + 10 + p_1(x-8)^2,$$
(A2)

and the second is the addition of a constant,

$$C = m(x-8) + 10 + p_2. (A3)$$

Again the Fisher matrix formalism is used to predict the future errors on the model parameters, (m, p_1) or (m, p_2) , given a configuration for the future data error bars.

The results are shown in Figs. A3 and A4. We show the errors on m (marginalised over p_i) and on p_i (marginalised over m). We could have constructed a figure of merit that combines the errors of m and p_i , but this is somewhat superfluous in this illustrative example.

In Fig. A3, we show how the errors on m and p_1 from model 1 are optimised. In this case, x=8 is a pivot point of the extended model so the optimal strategy is to maximise future errors at x=8 since the parameters are not sensitive to data at this point. The quadratic sum of the errors at x=4

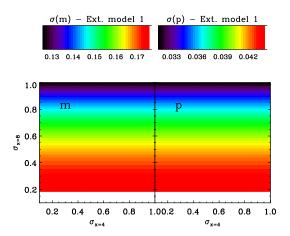


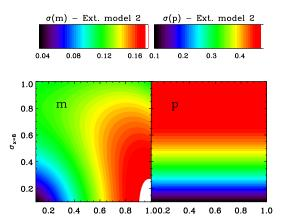
Figure A3. Optimisation for the two parameters of extended model 1, $C = m(x-8) + 10 + p_1(x-8)^2$. The plots show the expected marginalised errors on m and p_1 as a function of possible measurement errors at x=4 and x=8. As in Fig. A2, the errors at x=12 are set by fixing the quadratic sum of the errors to 2.01. For this extended model, we see that we are pushed to a configuration with maximum errors at x=8 for both parameters m and p_1 . As with the standard model, this extended model has a pivot point at x=8 and so the measurement here does not bring useful information. Unlike the example shown in Fig. A2, here the errors at both x=4 and 12 are important since they are both needed to distinguish between m and p_1 (with only one data point the two parameters are degenerate). This is why maximising the error at x=8, and hence minimising the quadratic sum at x=4 and 12, is preferred.

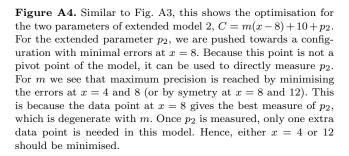
and 12 are then minimised. We note that in this example both of these data points are needed to distinguish between the parabolic and the linear term.

In Fig. A4, we show how the errors on m and p_2 from model 2 are optimised. In this extended model, x=8 is no longer a pivot point of the model. In fact, a small future error bar at x=8 could measure p_2 very accurately (for a given m) because the errors are not degenerate with m at this point. Hence, the optimisation places a small error bar at x=8. Next, to accurately measure m, the optimisation tries to minimise the errors on one of the two remaining errors in a similar way to what happen in Fig. A2.

A3 Breaking the Standard Model

For the Fisher matrix calculations we have made the implicit assumption that future measurement errors are Gaussian (Tegmark et al. 1997). For the model breaking approach, we make the same assumptions, namely that the probability of T given today's data is given by





$$P(T|X) = \exp\left(-\frac{(T-X)^2}{2\sigma_X^2}\right),\tag{A4}$$

where today's data vector is once again, $X = \{10, 10, 10\}$, and the probability of the future data given T is

$$P(Y|T) = \exp\left(-\frac{(Y-T)^2}{2\sigma_Y^2}\right). \tag{A5}$$

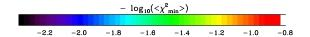
The future χ^2 is given simply by

$$\chi^2 = \sum_i \frac{1}{\sigma_{Y_i}^2} (C_i - Y_i)^2, \tag{A6}$$

which for the illustrative standard model used here (equation A1) is a minimum for

$$m = \frac{\sum_{i} \sigma_{i}^{-2} (x_{i} - 8)(10 - Y_{i})}{\sum_{i} \sigma_{i}^{-2} (x_{i} - 8)},$$
(A7)

where the sums are over $x=4,\,8,\,12.$ These allow us, for the simple model being considered here, to solve equation 4 analytically.



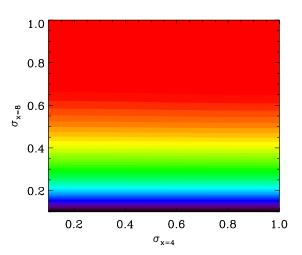


Figure A5. The expectation value of the future χ^2_{\min} . This expectation value must be maximised to have the best chance of breaking our standard model. The colour scheme for this plot has been chosen such that the best configuration $(\max(\langle \chi^2_{\min} \rangle))$ is purple (dark), which is consistent with Fig. A2 to A4 where the optimal strategies are also purple (dark). We see that using this criterion that the optimal configuration is one that minimises the errors at x=8. This can be understood since any deviation from $y\equiv 10$ at this point cannot be explained within our standard model. Given today's data and no guidance from theory, a high precision measurement here is, therefore, most likely to break the standard model.

Fig. A5 shows the result of the model breaking optimisation for this illustrative example. To have the best chance of breaking this standard model, one should place a very small error bar at x=8. This is understood since x=8 has a very stringent prediction that $C(x=8)\equiv 10$, any deviation from this prediction would be proof that the standard model was incorrect.

REFERENCES

Ahmed S. N., et al. 2004, Physical Review Letters, 92, 181301

Ahn M. H., et al 2006, Phys. Rev. D, 74, 072003

Albrecht A., Amendola L., Bernstein G., Clowe D., Eisenstein D., Guzzo L., Hirata C., Huterer D., Kirshner R., Kolb E., Nichol R., 2009, ArXiv e-prints

Albrecht A., Bernstein G., Cahn R., Freedman W. L., Hewitt J., Hu W., Huth J., Kamionkowski M., Kolb E. W., Knox L., Mather J. C., Staggs S., Suntzeff N. B., 2006, ArXiv Astrophysics e-prints

Amara A., Refregier A., 2004, MNRAS, 351, 375

Amara A., Réfrégier A., 2007, MNRAS, 381, 1018

Blake C., Parkinson D., Bassett B., Glazebrook K., Kunz M., Nichol R. C., 2006, MNRAS, 365, 255

Desjacques V., Seljak U., 2010, Classical and Quantum Gravity, 27, 124011

- Eguchi K., et al. 2003, Physical Review Letters, 90, 021802 Huterer D., Starkman G., 2003, Physical Review Letters, 90, 031301
- Huterer D., Turner M. S., 2001, Phys. Rev. D, 64, 123527Ishak M., Upadhye A., Spergel D. N., 2006, Phys. Rev. D, 74, 043513
- Kim A. G., Linder E. V., Miquel R., Mostek N., 2004, MN-RAS, 347, 909
- Kitching T., Amara A., Rassat A., Refregier A., 2009, ArXiv e-prints
- Kitching T. D., Amara A., 2009, MNRAS, 398, 2134
- Kitching T. D., Heavens A. F., Verde L., Serra P., Melchiorri A., 2008, Phys. Rev. D, 77, 103008
- Komatsu E., Dunkley J., Nolta M. R., Bennett C. L., Gold B., Hinshaw G., Jarosik N., Larson D., Limon M., Page L., Spergel D. N., Halpern M., Hill R. S., Kogut A., Meyer S. S., Tucker G. S., Weiland J. L., Wollack E., Wright E. L., 2009, ApJS, 180, 330
- Kowalski M., et al. 2008, ApJ, 686, 749
- Parkinson D., Blake C., Kunz M., Bassett B. A., Nichol R. C., Glazebrook K., 2007, MNRAS, 377, 185
- Percival W. J., et al 2010, MNRAS, 401, 2148
- Pillepich A., Porciani C., Hahn O., 2010, MNRAS, 402, 191
 Press W. H., Teukolsky S. A., Vetterling W. T., Flannery
 B. P., 2007, Numerical Recipes 3rd Edition: The Art of
 Scientific Computing. Cambridge University Press, New York, NY, USA
- Rassat A., Amara A., Amendola L., Castander F. J., Kitching T., Kunz M., Refregier A., Wang Y., Weller J., 2008, ArXiv e-prints
- Refregier A., Amara A., Kitching T., Rassat A., 2008, ArXiv e-prints
- Refregier A., Amara A., Kitching T. D., Rassat A., Scaramella R., Weller J., Euclid Imaging Consortium f. t., 2010, ArXiv e-prints
- Tegmark M., Eisenstein D. J., Hu W., Kron R., 1998, ArXiv Astrophysics e-prints
- Tegmark M., Taylor A. N., Heavens A. F., 1997, ApJ, 480, 22
- Thomas S. A., Abdalla F. B., Lahav O., 2009, ArXiv e-prints